# High Photocurrent Quantum Yields in Short Wavelengths for Nanocrystalline Anatase-Type $TiO_2$ Film Electrodes Compared with Those for Rutile-Type

**Akira Shiga, Akira Tsujiko, Shinji Yae, and Yoshihiro Nakato***

Department of Chemistry, Graduate School of Engineering Science,
and Research Center for Photoenergetics of Organic Materials, Osaka University, Toyonaka, Osaka 560-8531

(Received May 1, 1998)

Photoelectrochemical activity of nanocrystalline $TiO_2$ film electrodes prepared by use of various $TiO_2$ particles has been studied comparatively. It is confirmed that the photocurrent (or photoactivity) for anatase-type $TiO_2$ is in general higher than that for the rutile-type. The photocurrent quantum yield ($\eta_{pc}$) for anatase-type $TiO_2$ is nearly equal to that for rutile-type in long wavelengths but increases more and more with decreasing wavelength in contrast to the $\eta_{pc}$ for rutile-type, and thus the $\eta_{pc}$ for anatase-type becomes much higher than the $\eta_{pc}$ for rutile-type in short wavelengths around 300 nm, indicating that the high photoactivity for anatase-type $TiO_2$ is due to this high $\eta_{pc}$ in short wavelengths. There are some discussions on the reasons for the high $\eta_{pc}$ for anatase-type $TiO_2$ in short wavelengths, including the possibility of contribution of hot electrons or holes in the $TiO_2$ film.

Recently much attention has been paid to nanometer-sized (nanocrystalline) $TiO_2$ particles and their films from a point of view of cleaning of the environment by photocatalytic decomposition of waste materials, pollutants, harmful bacteria, etc.[1—17] They have also attracted growing attention in view of applications to dye sensitization solar cells[17—24] and electrochromic devices.[25,26] A number of basic studies have been made on the photocatalytic and photoelectrochemical properties (activity) of nanometer-sized $TiO_2$ particles and their films.[6,23,27—36]

The photoactivity of nanocrystalline $TiO_2$ films is in general governed by relative rates of various processes such as oxidation reactions by photogenerated holes at the $TiO_2$ surface, reduction reactions by photogenerated electrons at the $TiO_2$ surface, diffusion of the electrons and holes in the $TiO_2$ films, and various electron-hole recombination processes at the surface or in the bulk of $TiO_2$. The rates depend on particle size, crystal structure (anatase or rutile), impurities in particles, surface chemical structure or surface states, etc. In most studies reported thus far, the photoactivity has been measured by observing the kind and quantities of reaction products,[8—17] but by this method it is difficult to evaluate relative contributions of the above-mentioned various processes. The difficulty can be overcome to a large extent by measuring current–potential ($j$–$U$) curves for nanocrystalline $TiO_2$ film electrodes deposited on conductive substrates.

Of a number of studies reported on nanocrystalline $TiO_2$ film electrodes, most used anatase-type $TiO_2$. Nogami et al. compared the luminescent properties of anatase- and rutile-type $TiO_2$.[28] Augustynski et al. studied the $j$–$U$ curves for several anatase- and rutile-type $TiO_2$ in aqueous electrolytes with and without alcohol and oxygen.[30] We have studied the $j$–$U$ curves for several nanocrystalline $TiO_2$ (anatase and rutile) electrodes and reported that a Bardeen-type junction is formed as the main junction at the $TiO_2$/substrate interface.[37] In this work we will focus our attention on the photoactivity differences among various nanocrystalline $TiO_2$ film electrodes for the purpose of clarifying what are the main factors governing the photoactivity.

## Experimental

Five kinds of nanocrystalline $TiO_2$ film electrodes were used together with single crystal $n$-$TiO_2$ (rutile) electrodes. The main characteristics of the film electrodes, named film A, B, C, D, and E, are summarized in Table 1. A colloidal $TiO_2$ solution for film A was prepared by adding titanium tetrachloride to aqueous 1.0 M sodium carbonate (M = mol $dm^{-3}$), followed by addition of nitric acid, as described in the literature.[38] A colloidal $TiO_2$ solution for film B was prepared by adding a mixture of titanium tetra(isopropoxide) and 2-propanol to diluted nitric acid.[39] $TiO_2$ particles for films C, D, and E were supplied by the Catalysis Society of Japan. They are called TIO-3, TIO-4, and TIO-5, respectively, in the Society. The $TiO_2$ particles for film C are prepared by a liquid-phase method using titanium disulfate as the starting material, and those for films D and E are prepared by a gas-phase CVD method using titanium tetrachloride as the starting material. The $TiO_2$ particle for film D is essentially the same as what is called Degussa P-25. The $TiO_2$ powder for films C, D, and E was ground in a mortar with small amounts of water and acetylacetone, and the mixture was added to diluted $HNO_3$ under stirring, to obtain colloidal solutions.

Nanocrystalline $TiO_2$ film electrodes were prepared as follows:[37] Transparent conductive F-doped $SnO_2$ layers coated on glass plates (Nippon Sheet Glass Co., Ltd., sheet resistance ca. 20 Ω/square) were used as the substrate. They were washed successively with boiling acetone, 30% $HNO_3$, and pure water, and colloidal $TiO_2$ solutions were coated on them with a spin coater and heated at 150

Table 1. Main Characteristics of Nanocrystalline $TiO_2$ Films

| Film | Crystal structure (composition) | Particle size (nm) | Thickness (μm) | Appearances | Preparation method[a)] |
|---|---|---|---|---|---|
| A | 100% rutile | 10—30 | 0.25—0.35 | Transparent | $TiCl_4$ |
| B | 83% anatase + 17% rutile | 10—30 | 0.25—0.35 | Transparent | $Ti(OC_3H_7)_4$ |
| C | 100% rutile | 20—40 | 0.3—10 | Opaque | $Ti(SO_4)_2$ |
| D | 70% anatase + 30% rutile | 20—40 | ca. 1.2 | Opaque | $TiCl_4$ |
| E | 10% anatase + 90% rutile | 300—800 | 0.3—10 | Opaque | $TiCl_4$ |

a) See the Experimental section for details.

°C. This procedure was repeated several times and the $TiO_2$ films thus prepared were finally heated at 600 °C for 2 h in air. For reference, $TiO_2$ films prepared by thermal oxidation of Ti metal plates were investigated. The films were obtained by heating Ti metal plates at 600 °C for 1 h in air. Single crystal *n*-$TiO_2$ (rutile) electrodes were prepared by reduction of $TiO_2$ wafers in a hydrogen atmosphere at 600—700 °C. Other details were described elsewhere.[40)]

Current (*j*)–potential (*U*) curves were obtained with a commercial potentiostat and potential programmer, using a Pt plate as the counterelectrode and an Ag/AgCl/KCl(sat.) electrode as the reference electrode. Electrolyte solutions were prepared using deionized water and reagent grade chemicals without further purification. Nitrogen gas was bubbled through the electrolyte under stirring to remove dissolved oxygen in the solution. Illumination was done by white light from a 500-W Xe lamp (Ushio UXL-500). The light was passed through a water filter in a Pyrex glass cell, and was incident to the electrode from the front side (the $TiO_2$-film side). The electrolyte solution was kept at 25 °C during measurements.

The photocurrent quantum yields ($\eta_{pc}$) were obtained by measuring photocurrents at a sufficiently positive potential (+0.5 V vs. Ag/AgCl) where saturated (potential-independent) photocurrents were observed. Monochromatic light for electrode illumination was obtained with a Jahrel–Ash JE-25E monochromator and a 300-W Xe lamp (Ushio UXL-300) as the light source. The light was chopped at 0.5 Hz with a chopper (Scitec Instruments Ltd., 300HRG) such that the electrode was illuminated for 1 s every 2 s. The photocurrent vs. time curves, measured with a potentiostat and an *X*–*T* recorder, showed a rectangular shape with a steady photocurrent under illumination except an initial transient peak. The steady photocurrent was adopted for $\eta_{pc}$ calculation. The illumination intensity was measured with a thermopile (Eppley) every 5 nm throughout the wavelength range measured. The intensity was 0.38 mW $cm^{-2}$ at 340 nm.

UV absorption spectra for nanocrystalline $TiO_2$ films were obtained with a Shimadzu 2500PC spectrometer. For transparent films (films A and B, cf. Table 1), light transmittance was measured for films deposited on Pyrex glass plates, with a Pyrex glass plate as the reference. For opaque films, diffuse reflectance spectra were measured using an integral sphere attachment. In the latter case, the absorbance was obtained by using the Kubelka–Munk equation.

Inspection of electrode surfaces was done with a high resolution scanning electron microscope (Hitachi S-5000). X-ray diffraction (XRD) patterns were obtained with a Philips X'Pert diffractometer using a Cu $K\alpha$ ( = 1.5417 Å) radiation. The composition of anatase- and rutile-type in $TiO_2$ films was measured from peak areas of the characteristic XRD peak for each crystal structure by taking the reported composition for Degussa P-25 (film D)[31)] as a reference.

## Results

Scanning electron micrographs (SEM's) indicated that all $TiO_2$ films consisted of nanometer-sized particles, the size and the film thickness being summarized in Table 1. Films A and B were clear transparent films with well-packed particulate structure,[37)] while the other films, C, D, and E, prepared from commercial $TiO_2$ powder, had a coase structure. Especially, films C and E were not flat films but random arrays of μm-sized aggregates. In Table 1, crystal structure of $TiO_2$ particles obtained from X-ray diffraction patterns are also summarized.

Figure 1 shows UV absorption spectra for films A and B. Accurate spectra were obtained for these transparent films by light transmittance measurements as mentioned before, but only qualitative spectra were obtained for the other opaque films, C, D, and E, by measurements of diffuse reflectance spectra.

Figure 2 shows photocurrent (*j*) vs. potential (*U*) curves for rutile-type $TiO_2$ films, A and C, together with those for a single crystal *n*-$TiO_2$ (rutile) electrode. Solid curves are the *j*–*U* curves measured in $N_2$-bubbled 0.1 M $HClO_4$ (pH 1.1) and 0.1 M NaOH (pH 12.8), and broken curves are those measured in the solutions to which 0.31 M ethanol is

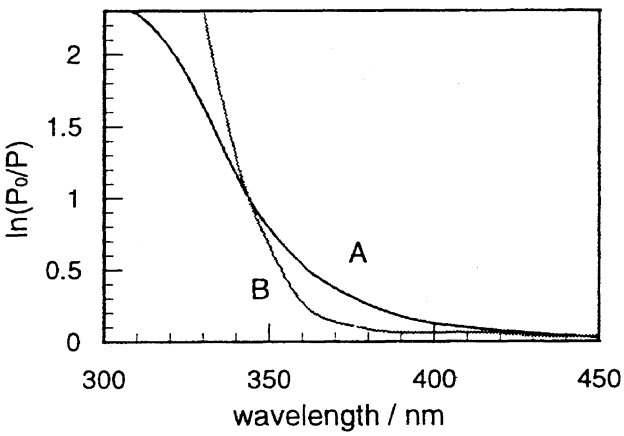


Fig. 1. UV absorption spectra for films A and B. Note that the ordinate is given by $\ln_e (P_0/P)$, not by $\log_{10} (P_0/P)$, where $P_0$ and $P$ are the incident and transmitted light intensities, respectively.

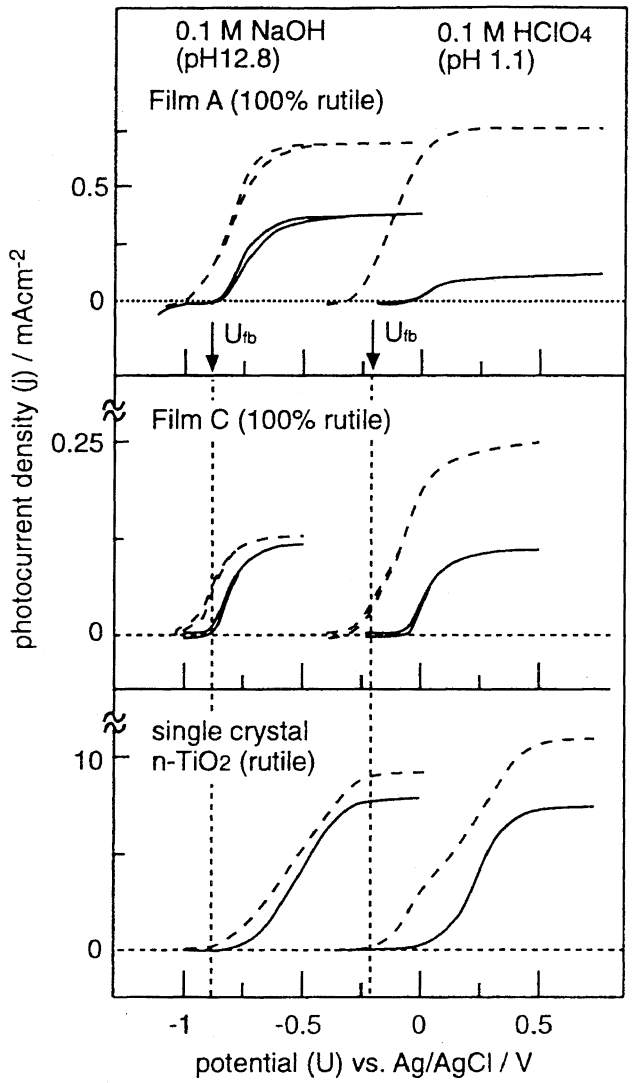


Fig. 2. Photocurrent ($j$) vs. potential ($U$) curves for rutile-type $TiO_2$ nanocrystalline film electrodes, together with those for a single crystal $n$-$TiO_2$ (rutile) electrode. Solid curves are for $N_2$-bubbled 0.1 M $HClO_4$ (pH 1.1) and 0.1 M NaOH (pH 12.8), and broken curves are for the solutions to which 0.31 M ethanol is added. $U_{fb}$ is the flat-band potential of single crystal $n$-$TiO_2$ (rutile) electrode,[41,42] corrected for solution-pH changes.

added (1 M = 1 mol dm$^{-3}$). The flat-band potential ($U_{fb}$) for single crystal $n$-$TiO_2$ (rutile)[41,42] is included in the figure with corrections for solution-pH changes at a ratio of 0.059 V/pH. As the $U_{fb}$ for single crystal $n$-$TiO_2$ is estimated to lie about 0.00 to 0.20 eV below the conduction-band edge at the surface ($E_c^s$), the $U_{fb}$ gives an indication for the $E_c^s$ of $TiO_2$ particles. All $TiO_2$ film electrodes show $j$–$U$ curves quite similar to those for single crystal $n$-$TiO_2$ electrodes (Fig. 2). In particular, the deviation ($\Delta U$) of the onset potential of photocurrent ($U_{on}$) from $U_{fb}$ ($\Delta U = U_{on} - U_{fb}$) in acidic solution (0.1 M $HClO_4$) without ethanol is, for all electrodes, much larger than that in alkaline solution (0.1 M NaOH). It is to be noted also that $\Delta U$ becomes nearly zero upon addition of ethanol to the solutions. The saturated photocurrent ($j_{sat}$) observed in sufficiently positive potentials is much increased by addition of ethanol, but the extent of the increase is different in different electrodes and solutions.

Figure 3 shows the $j$–$U$ curves for mixed anatase- and rutile-type $TiO_2$ films, B, D, and E, in $N_2$-bubbled 0.1 M $HClO_4$ (pH 1.1) and 0.1 M NaOH (pH 12.8) with and without 0.31 M ethanol, in the same way as in Fig. 2. The $U_{fb}$ for anatase-type $n$-$TiO_2$ single crystal electrodes[43] is included, which is ca. 0.20 V more negative than the $U_{fb}$ for rutile-type. Similar to Fig. 2, the deviation $\Delta U$ in acidic solution without ethanol is, for all electrodes, much larger than that in alkaline solution without ethanol. Also, the $\Delta U$ becomes nearly zero by addition of ethanol.

It is interesting to note here that the $j_{sat}$ in the presence

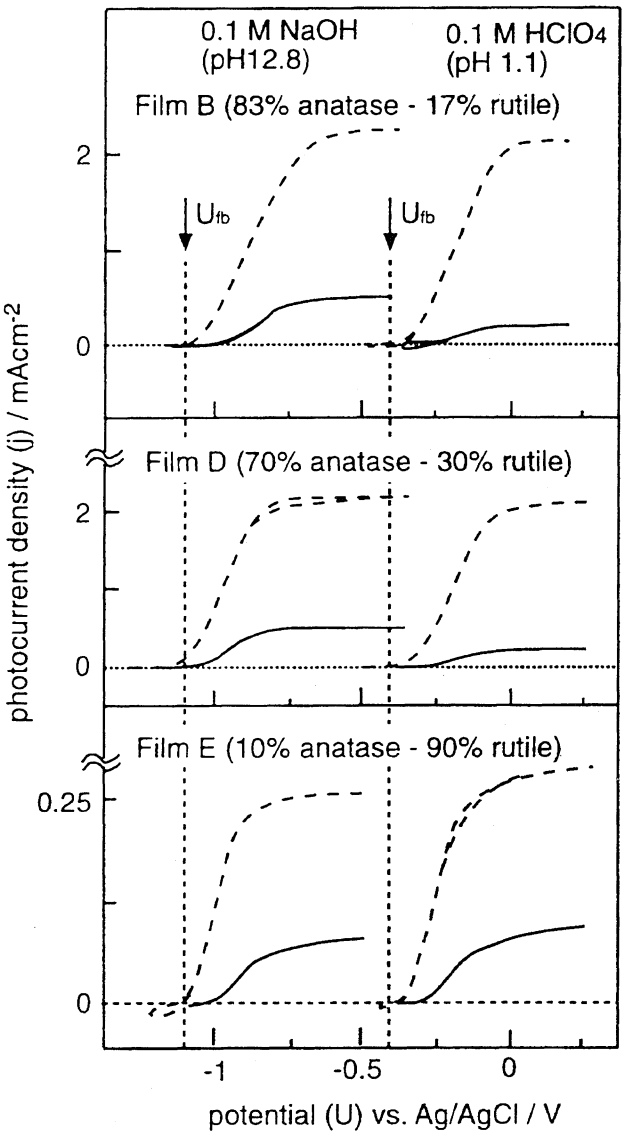


Fig. 3. The $j$–$U$ curves for mixed anatase- and rutile-type $TiO_2$ nanocrystalline film electrodes in $N_2$-bubbled 0.1 M $HClO_4$ (pH 1.1) and 0.1 M NaOH (pH 12.8) with and without 0.31 M ethanol, shown in the same way as in Fig. 2. $U_{fb}$ is the flat-band potential of anatase-type $n$-$TiO_2$ single crystal electrode.[43]

of ethanol for films B and D (Fig. 3), composed mainly of anatase-type $TiO_2$ is several times higher than the corresponding $j_{sat}$ for films A and C (Fig. 2), composed of 100% rutile-type $TiO_2$. Besides, the $j_{sat}$ in the presence of ethanol for the mixed anatase- and rutile-type $TiO_2$ films (films B, D, and E) in Fig. 3 decreases with decreasing percentage of anatase-type $TiO_2$. These results indicate that anatase-type $TiO_2$ in the presence of ethanol gives a much higher $j_{sat}$ than rutile-type $TiO_2$, and also that the $j$–$U$ curves for the mixed anatase- and rutile-type $TiO_2$ films in Fig. 3 are mainly given by anatase-type $TiO_2$ particles.

Figure 4 shows the $j$–$U$ curves for a $TiO_2$ (rutile) film prepared by thermal oxidation on a Ti-metal plate, displayed in the same way as in Figs. 2 and 3. The deviation $\Delta U$ is very large (about 0.3 V) both in acidic and alkaline solutions. The photocurrent gradually increases with the potential, showing almost no saturation. Moreover, no effect is observed by addition of 0.31 M ethanol, contrary to the case of nanocrystalline $TiO_2$ film electrodes.

Figure 5 shows the photocurrent quantum yields ($\eta_{pc}$) vs. illumination wavelength ($\lambda$) for films A and B in $N_2$-bubbled 0.1 M $HClO_4$ with and without 0.31 M ethanol, together with those for a single crystal $n$-$TiO_2$ (rutile) electrode. The $\eta_{pc}$ represents the photocurrent in the number of electrons against the number of absorbed photons, and is given by

$$\eta_{pc}(\lambda) = 1240 \times I(\lambda)/\lambda\, P_0(\lambda)[1 - P(\lambda)/P_0(\lambda)],$$

where $I(\lambda)$ is the photocurrent density in A cm$^{-2}$, and $P_0(\lambda)$ and $P(\lambda)$ are the incident and transmitted light intensities, respectively, in W cm$^{-2}$. The term $P(\lambda)/P_0(\lambda)$ can be calculated from the absorption spectra shown in Fig. 1. The effects of light reflection at the electrode surface on both the photocurrent ($I(\lambda)$) and light transmittance ($P(\lambda)/P_0(\lambda)$) are not corrected for in the $\eta_{pc}$ calculation. The $\eta_{pc}$ for film A (100% rutile) increases initially with decreasing $\lambda$ but begins to show a tendency to saturation at short $\lambda$, similar to the case of the single crystal $n$-$TiO_2$ (rutile) electrode. On

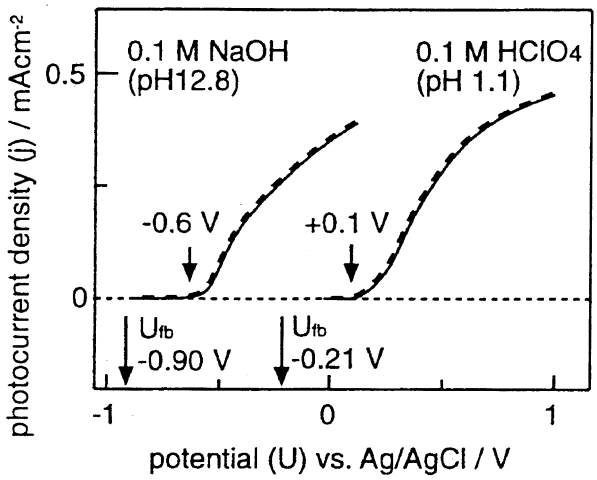


Fig. 4. The $j$–$U$ curves for a $TiO_2$ (rutile) film thermally grown on a Ti-metal plate, shown in the same way as in Figs. 2 and 3.

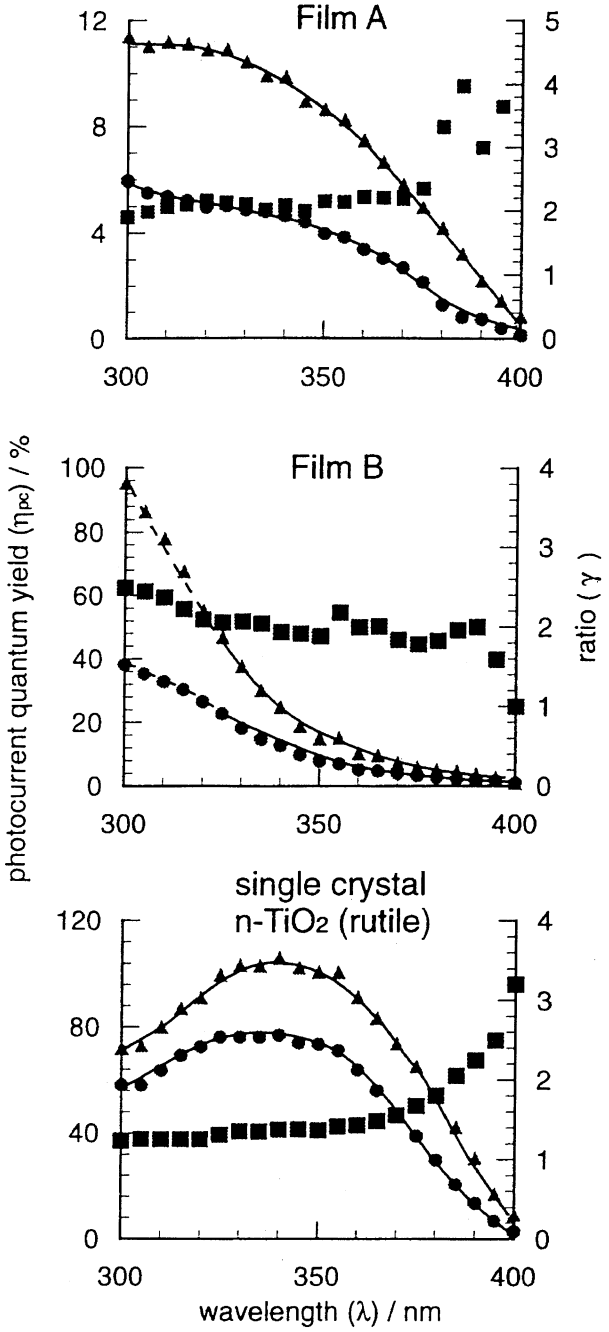


Fig. 5. Photocurrent quantum yields ($\eta_{pc}$) vs. illumination wavelength ($\lambda$) for films A and B in $N_2$-bubbled 0.1 M $HClO_4$ with and without 0.31 M ethanol, observed at 0.5 V vs. Ag/AgCl, together with those for a single crystal $n$-$TiO_2$ (rutile) electrode. ●: $\eta_{pc}$ in the absence of ethanol, ▲: $\eta_{pc}$ in the presence of ethanol, and ■: the ratio ($\gamma$) of the latter $\eta_{pc}$ to the former $\eta_{pc}$.

the other hand, the $\eta_{pc}$ for film B (83% anatase and 17% rutile) continues to increase with decreasing $\lambda$ even at short $\lambda$. Therefore, the $\eta_{pc}$ for film B is much higher than that for film A at around 300 nm (Note that the ordinate scale is different for films A and B in Fig. 5). The ratio of $\eta_{pc}$ in the presence of ethanol to that in the absence of ethanol is nearly constant with change in $\lambda$ for all electrodes, at least except

the region of $\lambda$ longer than ca. 370 nm.

## Discussion

The experimental results of Figs. 2 and 3 show that nanocrystalline $TiO_2$ film electrodes give $j$–$U$ curves well characterized by the onset potential ($U_{on}$) and the saturated photocurrent ($j_{sat}$). This means that the $U_{on}$ (or $\Delta U = U_{on} - U_{fb}$) and the $j_{sat}$ can be used as a measure of the photoelectrochemical activity of the electrodes. Augustynski et al. reported[30] that the photocurrent for rutile-type $TiO_2$ increased gradually with the potential, with large $\Delta U$, and was not affected by addition of alcohol (methanol), contrary to our results here. Their results for rutile-type $TiO_2$ seem to be rather similar to the results obtained for thermally grown $TiO_2$ (rutile) films (Fig. 4) in this work.

Let us first consider briefly the general features of the $j$–$U$ curves for nanocrystalline $TiO_2$ film electrodes. The deviation $\Delta U(=U_{on} - U_{fb})$ for water oxidation in acidic solution is large compared with that in alkaline solution (Figs. 2 and 3). Also, the $\Delta U$ becomes zero and the $j_{sat}$ is much increased by addition of alcohol to the solution. These features can be explained in terms of surface carrier recombination via intermediate radicals produced by oxidation reactions by photogenerated holes.

We reported in previous papers[44,45] that surface Ti–OH groups on single crystal $n$-$TiO_2$ (rutile) cannot be oxidized by photogenerated holes and thus, in acidic solutions, Ti–OH in some active sites such as atomic gaps is oxidized, resulting in relatively stable intermediate radicals (Ti·OH) in the active sites, which act as an effective recombination center. For such a case, photogenerated electrons can contribute to photocurrent only when certain band inclination (bending) is induced for $TiO_2$ under anodic bias. This mechanism leads to a large deviation $\Delta U$. Similar mechanism can be expected for nanocrystalline $TiO_2$ film electrodes. That the band inclination is induced for $TiO_2$ particles in direct contact with the substrate under anodic bias has been shown in our previous paper,[37] which reports that a Bardeen-type junction[46] is formed at the $TiO_2$-particle/substrate interface.

In alkaline solutions, an easily oxidized surface species such as Ti–$O^-$ is formed by deprotonation of surface Ti–OH groups (the point of zero charge for $TiO_2$ is ca. 5.5[47,48]) and is oxidized by holes, resulting in surface Ti–O· radicals. Such radicals are mobile and much more easily removed from the surface (followed by $O_2$ evolution) than the intermediate radicals in the active sites in acidic solutions. Thus, surface recombination via intermediate radicals in alkaline solutions becomes less efficient, leading to small $\Delta U$. The high $j_{sat}$ together with almost no deviation $\Delta U$ in alcohol-containing solutions can also be explained similarly, because the current-doubling mechanism for alcohol oxidation on $TiO_2$ results in less accumulation of surface intermediate radicals. Further details will be reported elsewhere.

Now let us consider the photoelectrochemical activity difference among various nanocrystalline $TiO_2$ film electrodes. The most pronounced difference is that the $j_{sat}$ for anatase-type $TiO_2$ in the presence of ethanol is several times higher than that for rutile-type $TiO_2$ films, as can be seen from comparison of Figs. 2 and 3. This result clearly shows that anatase-type $TiO_2$ is more active than the rutile-type. It should be noted here that the photocurrent quantum yield ($\eta_{pc}$) for anatase-type $TiO_2$ increases with decreasing wavelength ($\lambda$) and becomes much higher than that for rutile-type $TiO_2$ in short $\lambda$, especially in $\lambda$ shorter than 350 nm (Fig. 5). Thus we can conclude that the above high $j_{sat}$ (or photoactivity) for anatase-type $TiO_2$ is due to this high $\eta_{pc}$ for anatase-type $TiO_2$ in short $\lambda$.

The detailed mechanism at the high $\eta_{pc}$ for anatase-type $TiO_2$ in short $\lambda$ compared with that for rutile-type is unclear yet. In relation to this fact, it is also surprising that the $\eta_{pc}$ for nanocrystalline $TiO_2$ film electrodes, especially that for anatase-type $TiO_2$, increases with decreasing $\lambda$. Excitation in short $\lambda$ will produce hot electrons and hot holes having excess energies in the conduction and valence bands, respectively. However, if we assume that the hot electrons and holes were first thermalized in the bands (reaching the bottom of the conduction band and the top of the valence band respectively) and then caused various processes such as reduction or oxidation reactions, diffusion, and recombination, the $\eta_{pc}$ should be constant independent of $\lambda$, in disagreement with the experiments.

The $\eta_{pc}$ for single crystal $n$-$TiO_2$ electrodes shows $\lambda$-dependence (Fig. 5), which can be explained by a conventional mechanism[46] as follows. The light absorption coefficient of $TiO_2$ crystal increases with decreasing $\lambda$ and hence the light penetration depth decreases with decreasing $\lambda$. Thus, in long $\lambda$ with a long light penetration depth, a considerable part of the illuminated light is absorbed in a flat-band region beneath the space charge layer under anodic bias, and only a part of the holes generated in the flat-band region can reach the space charge layer and contribute to photocurrent, the other part recombining with conduction-band electrons in the flat-band region in the $TiO_2$ bulk. Thus, the $\eta_{pc}$ becomes higher as the light penetration depth gets smaller, i.e., $\lambda$ gets shorter, as really observed in a $\lambda$ range from 400 to 350 nm (Fig. 5). The observed $\eta_{pc}$ for single crystal $n$-$TiO_2$ shows a decrease with decreasing $\lambda$ in a $\lambda$ range shorter than 330 nm (Fig. 5). This can be explained by taking account of increased electron-hole recombination near the $n$-$TiO_2$ surface caused by large increases in the concentrations of photogenerated electrons and holes there due to too short light-penetration depths in short $\lambda$.

The above arguments for single crystal $n$-$TiO_2$ electrodes cannot, however, be applied to nanocrystalline $TiO_2$ electrodes, because the latter electrodes consist of very small $TiO_2$ particles, ca. 20 nm in diameter (Table 1), and the electrolyte penetrates into the electrodes down to the substrate.[37] For such nanocrystalline electrodes, we cannot assume the presence of a space charge layer. In addition, the illumination intensity within a $TiO_2$ particle will be nearly constant. We could rather say that the nanocrystalline $TiO_2$ electrodes resemble a suspension of $TiO_2$ particles in the electrolyte except that the $TiO_2$ particles are in contact with each other and electrons and holes can migrate between them. Thus, it is

quite difficult to understand the increased $\eta_{pc}$ in short $\lambda$ by the conventional mechanisms reported thus far. The consideration of the effect of light reflection at the electrode surface leads to decreased $\eta_{pc}$ in short $\lambda$, contrary to the experimental results, because the light reflectance increases with increasing absorption coefficient, i.e., decreasing $\lambda$. The consideration of the short light-penetration depth in short $\lambda$ also leads to low $\eta_{pc}$ in short $\lambda$ owing to increased carrier recombination in a surface region of the particulate electrode in the same way as mentioned for single crystal $n$-$TiO_2$ electrodes. There may be a certain inhomogeneity in inter-particle contact and electrolyte penetration for nanocrystalline $TiO_2$ electrodes. However, this does not seem to affect the $\lambda$-dependence of $\eta_{pc}$ for one electrode because the situation of each $TiO_2$ particle does not change with $\lambda$.

Thus, a possible explanation for the high $\eta_{pc}$ for anatase-type $TiO_2$ in the short $\lambda$ might be given by assuming that hot electrons or hot holes have certain mechanisms for less efficient carrier recombination or more efficient diffusion in the $TiO_2$ film. In this context, it may be interesting to note that Lévy et al. reported[49,50] that the electron mobility for anatase-type $TiO_2$ is much higher than that for rutile-type. Further studies are necessary to clarify the details.

This work was partly supported by a Grant-in-Aid for Scientific Research on Priority Area, "Electrochemistry of Ordered Interfaces" No. 09237105, from the Ministry of Education, Science, Sports and Culture.

## References

1) A. Fujishima and K. Honda, *Nature*, **238**, 37 (1972).
2) T. Inoue, A. Fujishima, S. Konishi, and K. Honda, *Nature*, **277**, 637 (1979).
3) R. Cai, K. Hashimoto, K. Itoh, Y. Kubota, and A. Fujishima, *Bull. Chem. Soc. Jpn.*, **64**, 1268 (1991).
4) "Photocatalysis - Fundamentals and Applications," ed by N. Serpone and E. Pellizzetti, Wiley, New York (1989).
5) "Photocatalytic Purification and Treatment of Water and Air," ed by D. F. Ollis and H. Al-Ekabi, Elsevier, Amsterdam (1993).
6) "Semiconductor Nanoclusters," ed by P. V. Kamat and D. Meisel, in "Studies in Surface Science and Catalysis," Elservier, Amsterdam (1996), Vol. 103.
7) M. A. Fox and M. T. Dulay, *Chem. Rev.*, **93**, 341 (1993).
8) M. R. Hoffmann, S. T. Martin, W. Choi, and D. W. Bahnemann, *Chem. Rev.*, **95**, 69 (1995).
9) A. L. Linsebigler, G. Lu, and J. T. Yates, Jr., *Chem. Rev.*, **95**, 735 (1995).
10) J. Schwitzgebal, J. G. Ekerdt, H. Gerischer, and A. Heller, *J. Phys. Chem.*, **99**, 5633 (1995).
11) K. Sayama and H. Arakawa, *J. Photochem. Photobiol. A: Chem.*, **77**, 243 (1994).
12) L. Sun and J. R. Bolton, *J. Phys. Chem.*, **100**, 4127 (1996).
13) A. Sclafani and J. M. Herrmann, *J. Phys. Chem.*, **100**, 13655 (1996).
14) M. Anpo, H. Yamashita, Y. Ichihashi, Y. Fujii, and M. Honda, *J. Phys. Chem. B*, **101**, 2632 (1997).
15) N. Takeda, M. Ohtani, T. Torimoto, S. Kuwabata, and H. Yoneyama, *J. Phys. Chem. B*, **101**, 2644 (1997).
16) B. Ohtani, K. Iwai, S. Nishimoto, and S. Sato, *J. Phys. Chem. B*, **101**, 3349 (1997).
17) D. W. Bahnemann, M. Hilgendorff, and R. Memming, *J. Phys. Chem. B*, **101**, 4265 (1997).
18) B. O'Regan and M. Grätzel, *Nature*, **335**, 737 (1991).
19) A. Hagfeldt and M. Grätzel, *Chem. Rev.*, **95**, 49 (1995).
20) K. Murakoshi, G. Kano, Y. Wada, S. Yanagida, H. Miyazaki, M. Matsumoto, and S. Murasawa, *J. Electroanal. Chem.*, **396**, 27 (1995).
21) F. Cao, G. Oskam, G. J. Meyer, and P. C. Searson, *J. Phys. Chem.*, **100**, 17021 (1996).
22) R. Grünwald and H. Tributsch, *J. Phys. Chem. B*, **101**, 2564 (1997).
23) A. Zaban, A. Meier, and B. A. Gregg, *J. Phys. Chem. B*, **101**, 7985 (1997).
24) G. Schlichthörl, S. Y. Huang, J. Sprague, and A. J. Frank, *J. Phys. Chem. B*, **101**, 8141 (1997).
25) C. G. Granqvist, "Handbook of Inorganic Electrochromic Materials," Elsevier, Amsterdam (1995), Chap. 15.
26) C. Bechinger, S. Ferrere, A. Zaban, J. Sprague, and B. A. Gregg, *Nature*, **383**, 608 (1996).
27) S. Södergren, H. Siegbahn, H. Rensmo, H. Lindström, A. Hagfeldt, and S. -E. Lindquist, *J. Phys. Chem. B*, **101**, 3087 (1997).
28) Y. Hamasaki, S. Ohkubo, K. Murakami, H. Sei, and G. Nogami, *J. Electrochem. Soc.*, **141**, 660 (1994).
29) S. Södergren, A. Hagfeldt, J. Olsson, S. -E. Lindquist, *J. Phsy. Chem.*, **98**, 5552 (1994).
30) A. Wahl, M. Ulmann, A. Carroy, B. Jermann, M. Dolata, P. Kedzierzawski, C. Chatelain, A. Monnier, and J. Augustynski, *J. Electroanal. Chem.*, **396**, 41 (1995).
31) F. Cao, G. Oskam, P. C. Searson, J. M. Stipkala, T. A. Heimer, F. Farzad, and G. J. Meyer, *J. Phys. Chem.*, **99**, 11974 (1995).
32) I. D. Makuta, S. K. Poznyak, and A. I. Kulak, *Electrochim. Acta*, **40**, 1761 (1995).
33) H. Rensmo, H. Lindström, S. Södergren, A. -K. Willstedt, A. Hagfeldt, and S. -E. Lindquist, *J. Electrochem. Soc.*, **143**, 3173 (1996).
34) T. Torimoto, R. J. Fox, and M. A. Fox, *J. Electrochem. Soc.*, **143**, 3712 (1996).
35) G. K. Boschloo, A. Goossens, and J. Schoonman, *J. Electroanal. Chem.*, **428**, 25 (1997).
36) P. E. de Jongh and D. Vanmaekelbergh, *J. Phys. Chem. B*, **101**, 2716 (1997).
37) A. Shiga, A. Tsujiko, T. Ide, S. Yae, and Y. Nakato, *J. Phys. Chem. B*, in press.
38) I. Sopyan, M. Watanabe, S. Murasawa, K. Hashimoto, and A. Fujishima, *Chem. Lett.*, **1996**, 69.
39) B. O'Regan, J. Moser, M. Anderson, and M. Grätzel, *J. Phys. Chem*, **94**, 8720 (1990).
40) Y. Nakato, H. Akanuma, J. -I. Shimizu, and Y. Magari, *J. Electroanal. Chem.*, **396**, 35 (1995).
41) M. Butler and D. S. Ginley, *J. Electrochem. Soc.*, **125**, 228 (1978).
42) M. J. Tomkiewicz, *J. Electrochem. Soc.*, **126**, 1505 (1979).
43) L. Kavan, M. Grätzel, S. E. Gilbert, C. Klemenz, and H. J. Scheel, *J. Am. Chem. Soc.*, **118**, 6716 (1996).
44) Y. Magari, H. Ochi, S. Yae, and Y. Nakato, "ACS Symp. Series, No. 656 (Solid/Liquid Electrochemical Interfaces)," American Chemical Society, Washington, D.C. (1996), Chap. 21, p. 297.
45) Y. Nakato, H. Akanuma, Y. Magari, S. Yae, J. -I. Shimizu,

and H. Mori, *J. Phys. Chem. B*, **101**, 4934 (1997).
46) S. M. Sze, "Physics of Semiconductor Devices," 2nd ed, John-Wiely & Sons, New York (1981).
47) M. A. Butler and D. S. Ginley, *J. Electrochem. Soc.*, **125**, 228 (1978).
48) D. E. Yates, R. O. James, and T. W. Healy, *J. Chem. Soc., Faraday Trans. 1*, **76**, 1 (1980).
49) L. Forro, O. Chauvet, D. Emin, L. Zuppiroli, H. Berger, and F. Lévy, *J. Appl. Phys.*, **75**, 633 (1994).
50) H. Tang, K. Prasad, R. Sanjinès, P. E. Schmid, and F. Lévy, *J. Appl. Phys.*, **75**, 2042 (1994).